Queensland University of Technology
Brisbane Australia

This is the author's version of a work that was submitted/accepted for publication in the following source:

Johnston, Stuart, Simpson, Matthew, & Baker, Ruth (2012) Mean-field descriptions of collective migration with strong adhesion. *Physical Review E*, *85*(5), 051922-1 .

This file was downloaded from: http://eprints.qut.edu.au/50414/

© Copyright 2012 American Physical Society

Notice: *Changes introduced as a result of publishing processes such as copy-editing and formatting may not be reflected in this document. For a definitive version of this work, please refer to the published source:*

http://dx.doi.org/10.1103/PhysRevE.85.051922

Drafted for *Physical Review E* , May 11, 2012

Mean-field descriptions of collective migration with strong adhesion

Stuart T Johnston[1], Matthew J Simpson[1,2], Ruth E Baker[3]

[1]*School of Mathematical Sciences, Queensland University of Technology, Brisbane, Australia.*

[2]*Tissue Repair and Regeneration Program,*

Institute of Health and Biomedical Innovation (IHBI),

Queensland University of Technology, Brisbane, Australia. and

[3]*Centre for Mathematical Biology, Mathematical Institute,*

University of Oxford, 24-29 St Giles', Oxford, OX1 3LB, UK.

Abstract

Random walk models based on an exclusion process with contact effects are often used to represent collective migration where individual agents are affected by agent-to-agent adhesion. Traditional mean-field representations of these processes take the form of a nonlinear diffusion equation which, for strong adhesion, does not predict the averaged discrete behavior. We propose an alternative suite of mean-field representations, showing that collective migration with strong adhesion can be accurately represented using a moment closure approach.

PACS numbers: 87.17.Rt 87.17.Jj

Keywords: cell migration, cell adhesion, Kirkwood superposition approximation, moment closure approximation

I. INTRODUCTION

Microscopic transport processes modulated by adhesion are important for many applications including the study of biomolecules [1], granular media [2] and biological cells [3, 4]. For these applications it is essential to understand how individual-level details of the adhesion mechanism lead to population-level properties that govern system-wide behavior. Therefore, accurate mean-field models of these mechanisms are essential. Here, we study a discrete motility mechanism based on an exclusion process [5] with contact effects. These models have been used to study migration of glioma cells [6, 7], breast cancer cells [8] and wound healing processes [9]. Anguige and Schmieser [10] were the first to derive a mean-field description of such a discrete model, with others reported subsequently [6, 8, 11, 12]. These previous studies reported mean-field representations in the form of a nonlinear diffusion partial differential equation (pde) [12].

The form of the nonlinear diffusivity function reflects the physical behavior in the discrete model [10–12]. When contact enhances migration, the nonlinear diffusivity function is always positive [6, 11, 13, 14]. When contacts reduce migration (i.e. adhesion) the nonlinear diffusivity function can become negative when contact effects dominate [8, 10, 11]. The transition from positive to negative nonlinear diffusivity is associated with clustering in the discrete simulations [13]; under these conditions existing mean-field models do not predict the average behavior of the discrete process [6, 11, 13]. For example, both Deroulers et al. [6] and Fernando et al. [11] showed that the traditional mean-field pde fails to make accurate predictions when contact effects became sufficiently strong. Fernando et al. [11] provided further insight by proposing a heuristic measure to predict the parameter regime where the mean-field pde was either accurate or inaccurate. Although insightful, this previous study provided no means of making accurate mean-field predictions when contact effects were strong.

Currently, is impossible to quantify how and why the traditional pde representation fails to predict the averaged discrete behavior as these models provide no way of examining the validity of the assumptions underlying the traditional mean-field pde. Here we address these issues by showing that an adhesive motility mechanism can be described by a suite of three mean-field models. We show that the traditional pde invokes two key assumptions, namely:

1. that effects of $\mathcal{O}(\Delta^3)$ and smaller are neglected in the limit that $\Delta \to 0$, where Δ is the lattice spacing, and

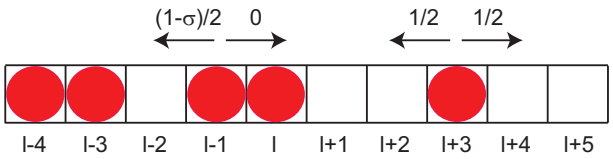

FIG. 1: (Color online). The random walk takes place on a one-dimensional lattice where each site can be occupied by, at most, one agent. An isolated agent steps in the positive or negative x direction with probability $1/2$ per computational time step. For example, the agent at site $l+3$ would step to site $l+2$ with probability $1/2$, or to $l+4$ with probability $1/2$. Contact effects alter the motility probability, for example in the configuration shown, the agent at site $l-1$ would step to $l-2$ with probability $(1-\sigma)/2$, where $\sigma \in [-1,1]$ represents the contact effect. The agent at site $l-1$ would step to site l with probability 0 since the target site is occupied.

2. the occupancy status of lattice sites are assumed to be independent so that correlation effects are ignored.

Two alternative mean-field models are developed that relax both these assumptions independently. Comparing averaged discrete simulation results to the predictions of the suite of three mean-field models highlights the role of correlation effects and shows that it is possible to make accurate mean-field predictions with strong adhesion using a moment closure approach.

II. DISCRETE MECHANISM

We consider a one-dimensional lattice, with spacing Δ. Sites are indexed by l, and have location $x = l\Delta$. Time is uniformly discretized with time step τ, and a random sequential update method is used to simulate the process [15]. During each time step, agents attempt to step to nearest neighbor sites provided that the target site is vacant. Motility events that would place an agent on an occupied site are aborted. Motility events are regulated by contact effects that represent agent-to-agent adhesion [10] by altering the motility using an adhesion parameter $\sigma \in [-1,1]$. For example, if we consider the schematic illustration in Figure 1, the agent at site $l-1$ would attempt to move to the vacant site $l-2$ with probability $(1-\sigma)/2$ per time step when site l is occupied. Alternatively, this event would occur with probability $1/2$ per time step if site l were vacant. Setting $\sigma > 0$ represents adhesion, whereas setting $\sigma < 0$ represents repulsion [11].

III. MEAN FIELD REPRESENTATIONS

We define the lattice variable, $\phi_l \in \{0_l, C_l\}$, to represent the state of the l^{th} site, so that $\phi_l = 0_l$ indicates that site l is vacant and $\phi_l = C_l$ indicates that site l is occupied. Averaging the occupancy

of each site over many identically prepared realizations gives $c_l \in [0,1]$ [6, 11]. In our notation upper case C_l represents the occupancy of the l^{th} site in a single realization, whereas lower case c_l represents the average occupancy, where the average is constructed over a large number of identically prepared realizations of the same process. We now introduce three ways to approximate c_l by making different assumptions about the underlying discrete process.

A. Partial differential equation representation

To connect the discrete mechanism with a pde, we form a discrete conservation statement describing δc_l, the change in average occupancy of site l per time step. The conservation equation can be written as

$$\begin{aligned}\delta c_l \;=\; & \frac{1}{2}\left[c_{l-1}(1-c_l)(1-\sigma c_{l-2})\right.\\ & \left.+c_{l+1}(1-c_l)(1-\sigma c_{l+2})\right]\\ & -\frac{1}{2}\left[c_l(1-c_{l-1})(1-\sigma c_{l+1})\right.\\ & \left.+c_l(1-c_{l+1})(1-\sigma c_{l-1})\right], \end{aligned} \tag{1}$$

where positive terms on the right of equation (1) represent events that would place agents at site l, and negative terms represent events that would remove agents from site l. The discrete conservation statement is related to a pde as $\Delta \to 0$ and $\tau \to 0$, and c_l is identified as a continuous variable $c(x,t)$ [6, 10, 11]. Expanding all terms in equation (1) in a truncated Taylor series about site l, neglecting terms of $\mathcal{O}(\Delta^3)$ and higher [6, 10, 11], and dividing the resulting expression by τ, we take limits as $\Delta \to 0$ and $\tau \to 0$ with the ratio (Δ^2/τ) held constant [16] to obtain

$$\frac{\partial c}{\partial t} = D_0 \frac{\partial}{\partial x}\left[D(c)\frac{\partial c}{\partial x}\right], \tag{2}$$

where $D_0 = \lim_{\Delta,\tau\to 0}(\Delta^2)/(2\tau)$ is the free-agent diffusivity, and the nonlinear diffusivity function is given by [10, 11]

$$D(c) = 1 - \sigma c(4-3c). \tag{3}$$

Two key assumptions lead to equation (2). First, we assume terms of $\mathcal{O}(\Delta^3)$ and smaller can be neglected. Second, we assume the average occupancies of sites to be independent so that, for example, the net averaged probability of a transition from site l to $l+1$ is proportional to $(1-c_{l+1})(1-\sigma c_{l-1})$. This implies that the occupancy of sites $l+1$ and $l-1$ are independent

which, in general, is untrue [17, 18]. Without further analysis, it is impossible to deduce how these two assumptions control the net error associated with equation (2). We now introduce two alternative mean-field models that systematically relax both assumptions.

B. Ordinary differential equation representation

To avoid neglecting terms of $\mathcal{O}(\Delta^3)$ and smaller as $\Delta \to 0$, we retain the spatial structure of the random walk in equation (1) by identifying discrete values of c_l with a continuous variable $c_l(t)$. Dividing equation (1) by τ, and considering the limit as $\tau \to 0$, gives a system of ordinary differential equations (odes)

$$\begin{aligned}\frac{\mathrm{d}c_l}{\mathrm{d}t} &= \frac{1}{2}\left[c_{l-1}(1-c_l)(1-\sigma c_{l-2})\right.\\ &\quad \left.+c_{l+1}(1-c_l)(1-\sigma c_{l+2})\right]\\ &\quad -\frac{1}{2}\left[c_l(1-c_{l-1})(1-\sigma c_{l+1})\right.\\ &\quad \left.+c_l(1-c_{l+1})(1-\sigma c_{l-1})\right], \end{aligned} \tag{4}$$

for each site l. We note that equation (4) still makes the independence assumption, and we now develop a third mean-field model that removes this assumption.

C. Moment closure representation

We use k-point distribution functions, $\rho^{(k)}$ $(k = 1, 2, 3\ldots)$, to describe the averaged occupancies of k-tuplets of lattice sites [17, 19, 20]. For $k = 1$, the distribution function is a univariate distribution describing the average density of agents on site l so that $\rho^{(1)}(C_l) = c_l$. For $k = 2$, the bivariate distribution function can be defined in terms of correlation functions [17, 19], which can be written as

$$F(l, m) = \frac{\rho^{(2)}(C_l, C_m)}{\rho^{(1)}(C_l)\rho^{(1)}(C_m)}, \tag{5}$$

where $l \neq m$. These correlation functions allow us to relax the independence assumptions inherent in equations (2) and (4). Setting $F(l, m) \equiv 1$ indicates that the occupancies of sites l and m are independent. Instead, we avoid this assumption by allowing $F(l, m)$ to evolve as part of the

solution [17]. With these definitions we have

$$\begin{aligned}\frac{\mathrm{d}c_l}{\mathrm{d}t} &= \frac{1}{2}\left[\rho^{(3)}(0_{l-2}, C_{l-1}, 0_l) + (1-\sigma)\rho^{(3)}(C_{l-2}, C_{l-1}, 0_l)\right] \\ &+\frac{1}{2}\left[\rho^{(3)}(0_l, C_{l+1}, 0_{l+2}) + (1-\sigma)\rho^{(3)}(0_l, C_{l+1}, C_{l+2})\right] \\ &-\frac{1}{2}\left[\rho^{(3)}(0_{l-1}, C_l, 0_{l+1}) - (1-\sigma)\rho^{(3)}(0_{l-1}, C_l, C_{l+1})\right] \\ &-\frac{1}{2}\left[\rho^{(3)}(0_{l-1}, C_l, 0_{l+1}) - (1-\sigma)\rho^{(3)}(C_{l-1}, C_l, 0_{l+1})\right]. \end{aligned} \tag{6}$$

Positive terms on the right of equation (6) represent events that would place an agent at site l whereas negative terms on the right of equation (6) represent events that would remove an agent from site l. To simplify equation (6) we apply a summation rule [17] to rewrite the unbiased $\rho^{(3)}$ terms as equivalent $\rho^{(2)}$ terms. The Kirkwood Superposition Approximation (KSA) is then used to rewrite the remaining $\rho^{(3)}$ terms as combinations of of $\rho^{(2)}$ terms. The KSA is a moment closure approximation that has been used in many applications including ecology [21–23], physical chemistry [24], disease biology [25, 26] and diffusion-mediated reactions [27]. The KSA can be written as

$$\rho^{(3)}(\phi_l, \phi_m, \phi_n) = \frac{\rho^{(2)}(\phi_l, \phi_m)\rho^{(2)}(\phi_l, \phi_n)\rho^{(2)}(\phi_m, \phi_n)}{\rho^{(1)}(\phi_l)\rho^{(1)}(\phi_m)\rho^{(1)}(\phi_n)}. \tag{7}$$

Combining equation (7) with the simplified version of equation (6) gives

$$\begin{aligned}\frac{\mathrm{d}c_l}{\mathrm{d}t} &= \frac{1}{2}\left[c_{l+1} - 2c_2 + c_{l-1}\right] \\ &- \frac{\sigma}{2(1-c_l)}\left[c_{l-2}c_{l-1}(1 - c_l F(l-2, l)) \right. \\ &\left.(1 - c_l F(l-1, l))F(l-2, l-1)\right] \\ &- \frac{\sigma}{2(1-c_l)}\left[c_{l+1}c_{l+2}(1 - c_l F(l, l+1)) \right. \\ &\left.(1 - c_l F(l, l+2))F(l+1, l+2)\right] \\ &+ \frac{\sigma}{2(1-c_{l-1})}\left[c_l c_{l+1}(1 - c_{l-1} F(l-1, l)) \right. \\ &\left.(1 - c_{l-1} F(l-1, l+1))F(l, l+1)\right] \\ &+ \frac{\sigma}{2(1-c_{l+1})}\left[c_{l-1}c_l(1 - c_{l+1} F(l-1, l+1)) \right. \\ &\left.(1 - c_{l+1} F(l, l+1))F(l, l-1)\right]. \end{aligned} \tag{8}$$

To solve equation (8) we require a model for the evolution of $F(l,l+1)$ and $F(l,l+2)$ which are correlation functions quantifying the degree to which the occupancy of the pairs of sites, $(l,l+1)$ and $(l,l+2)$, are correlated. To solve for these terms we consider the time rate of change of certain 2-point distribution functions which are related to higher order distribution functions leading to an infinite system of equations that we close using the KSA [17, 18]. For example, the evolution of $\rho^{(2)}(C_l, C_{l+1})$ is given by

$$\begin{aligned}\frac{\mathrm{d}\rho^{(2)}(C_l,C_{l+1})}{\mathrm{d}t} &= \frac{1}{2}\left[\rho^{(4)}(0_{l-2},C_{l-1},0_l,C_{l+1})+(1-\sigma)\rho^{(4)}(C_{l-2},C_{l-1},0_l,C_{l+1})\right]\\ &+\frac{1}{2}\left[\rho^{(4)}(C_l,0_{l+1},C_{l+2},0_{l+3})+(1-\sigma)\rho^{(4)}(C_l,0_{l+1},C_{l+2},0_{l+3})\right]\\ &-\frac{1}{2}\left[(1-\sigma)\rho^{(3)}(0_{l-1},C_l,C_{l+1})+(1-\sigma)\rho^{(3)}(C_l,C_{l+1},0_{l+2})\right]. \end{aligned} \tag{9}$$

To simplify equation (9) we apply a summation rule [17] to rewrite the unbiased $\rho^{(4)}$ terms as equivalent $\rho^{(3)}$ terms. Then, we use the summation rule again to write some of the resulting $\rho^{(3)}$ terms as equivalent expressions depending only on $\rho^{(2)}$ terms. This gives us

$$\begin{aligned}\frac{\mathrm{d}\rho^{(2)}(C_l,C_{l+1})}{\mathrm{d}t} &= \frac{1}{2}\left[\rho^{(2)}(C_{l-1},C_{l+1})+\rho^{(2)}(C_l,C_{l+2})-2\rho^{(2)}(C_l,C_{l+1})\right]\\ &-\frac{\sigma}{2}\left[\rho^{(4)}(C_{l-2},C_{l-1},0_l,C_{l+1})+\rho^{(4)}(C_l,0_{l+1},C_{l+2},C_{l+3})\right]\\ &+\frac{\sigma}{2}\left[\rho^{(3)}(0_{l-1},C_l,C_{l+1})+\rho^{(3)}(C_l,C_{l+1},0_{l+2})\right]. \end{aligned} \tag{10}$$

We now use the KSA to reduce the $\rho^{(3)}$ and $\rho^{(4)}$ terms in equation (10). For the $\rho^{(4)}$ terms we use [24]

$$\rho^{(4)}(\phi_l,\phi_m,\phi_n,\phi_o) = \frac{\rho^{(3)}(\phi_l,\phi_m,\phi_n)\rho^{(3)}(\phi_l,\phi_m,\phi_o)\rho^{(3)}(\phi_l,\phi_n,\phi_o)\rho^{(3)}(\phi_m,\phi_n,\phi_o)\rho^{(1)}(\phi_l)\rho^{(1)}(\phi_m)\rho^{(1)}(\phi_n)\rho^{(1)}(\phi_o)}{\rho^{(2)}(\phi_l,\phi_m)\rho^{(2)}(\phi_l,\phi_n)\rho^{(2)}(\phi_l,\phi_o)\rho^{(2)}(\phi_m,\phi_n)\rho^{(2)}(\phi_m,\phi_o)\rho^{(2)}(\phi_n,\phi_o)}. \tag{11}$$

The $\rho^{(3)}$ terms appearing in equation (11) can then be reduced into $\rho^{(2)}$ terms using equation (7).

At this stage there are two possible ways to simplify equation (10). Either we:

1. introduce the KSA directly into equation (10) to express the $\rho^{(3)}$ and $\rho^{(4)}$ terms as $\rho^{(2)}$ terms or,

2. apply the summation rule again to further simplify those terms in equation (10) that are proportional to σ.

Following the second approach we obtain

$$\begin{aligned}\frac{\mathrm{d}\rho^{(2)}(C_l, C_{l+1})}{\mathrm{d}t} &= \frac{1}{2}\left[\rho^{(2)}(C_{l-1}, C_{l+1}) + \rho^{(2)}(C_l, C_{l+2}) - 2\rho^{(2)}(C_l, C_{l+1})\right] \\ &-\frac{\sigma}{2}\left[\rho^{(2)}(C_{l-1}, C_{l+1}) + \rho^{(2)}(C_l, C_{l+2}) - 2\rho^{(2)}(C_l, C_{l+1})\right] \\ &+\frac{\sigma}{2}\left[\rho^{(4)}(0_{l-2}, C_{l-1}, 0_l, C_{l+1}) + \rho^{(4)}(C_l, 0_{l+1}, C_{l+2}, 0_{l+3})\right]. \qquad (12)\end{aligned}$$

We apply the KSA to equation (12) and rewrite everything in terms of the correlation functions to obtain

$$\begin{aligned}&\frac{\mathrm{d}F(l,l+1)}{\mathrm{d}t} = -F(1,1+1)\left[\frac{\mathrm{d}c_{l+1}}{\mathrm{d}t}\frac{1}{c_{l+1}} + \frac{\mathrm{d}c_l}{\mathrm{d}t}\frac{1}{c_l}\right] \\ &+\frac{1}{2}\left[\frac{c_{l-1}}{c_l}F(l-1,l+1) + \frac{c_{l+2}}{c_{l+1}}F(l,l+2) - 2F(l,l+1)\right] \\ &-\frac{\sigma}{2}\left[\frac{c_{l-1}}{c_l}F(l-1,l+1) + \frac{c_{l+2}}{c_{l+1}}F(l,l+2) - 2F(l,l+1)\right] \\ &+\frac{\sigma}{2}\left[\frac{c_{l-1}}{c_l(1-c_{l-2})^2(1-c_l)^2}F(l-1,l+1)\left[1-c_{l-2}-c_l+c_lc_{l-2}F(l-2,l)\right]\right. \\ &\left.\left[1-c_{l-2}F(l-2,l-1)\right]\left[1-c_{l-2}F(l-2,l+1)\right]\left[1-c_lF(l-1,l)\right]\left[1-c_lF(l,l+1)\right]\right] \\ &+\frac{\sigma}{2}\left[\frac{c_{l+2}}{c_{l+1}(1-c_{l+1})^2(1-c_{l+3})^2}F(l,l+2)\left[1-c_{l+1}-c_{l+3}+c_{l+1}c_{l+3}F(l+1,l+3)\right]\right. \\ &\left.\left[1-c_{l+1}F(l,l+1)\right]\left[1-c_{l+3}F(l,l+3)\right]\left[1-c_{l+1}F(l+1,l+2)\right]\left[1-c_{l+3}F(l+2,l+3)\right]\right] \qquad (13)\end{aligned}$$

To solve the moment closure model we use the same initial condition, $c(x,0)$, as in the discrete simulations and set the initial values of $F(l,m) \equiv 1$, for all $m = l+1, l+2, l+3...$ and for all all lattice sites l [18]. While it is possible, in principle, to solve $F(l,m)$ for all values of m to cover the periodic domain, it is more practical to solve a truncated system $F(l,m)$ for $m = l+1, l+2, ..., M$ assuming that $F(l, M+1) \equiv 1$. We did this iteratively by solving for c_l, $F(l,l+1)$ and setting $F(l,l+2) \equiv 1$, and then solving for c_l, $F(l,l+1)$, $F(l,l+2)$ and setting $F(l,l+3) \equiv 1$. These two approaches yielded results for $c(x,t)$ that were indistinguishable. Therefore, we take the simplest possible approach and report results corresponding to the solution of c_l and $F(l,l+1)$ with $F(l,l+2) \equiv 1$. We also remark that, as we pointed out earlier, it is possible to simplify equation (10) in an alternative way by applying the KSA directly to the $\rho^{(3)}$ and $\rho^{(4)}$ terms in that equation without using the summation rule. For completeness, we also resolved all problems in this work using the alternative expression for $\mathrm{d}F(l,l+1)/\mathrm{d}t$ and found that both approaches yielded $c(x,t)$ profiles that were indistinguishable.

IV. RESULTS AND DISCUSSION

We consider a lattice with $1 \leq x \leq 1000$, and an initial distribution of agents given by

$$c(x,0) = \begin{cases} 0.1, & 1 \leq x < 480\,, \\ 1.0, & 481 \leq x \leq 520\,, \\ 0.1, & 521 < x \leq 1000\,. \end{cases} \tag{14}$$

Periodic boundary conditions are imposed, and simulations are performed for a range of σ including $(-1.00, -0.95, -0.90 \ldots 0.90, 0.95, 1.00)$. In each case we estimate the density profile using 1000 identically prepared realizations. Results in Figures 2–3 are given at $t = 1000$ and $t = 5000$, respectively. Snapshots are shown for modest ($\sigma = 0.65$), strong ($\sigma = 0.80$) and extreme ($\sigma = 0.95$) adhesion. We show 20 identically-prepared realizations of the same stochastic process which illustrate the effects of adhesion since clustering occurs when adhesion dominates (Figure 2–3 (b)). The density profiles in the central region of the lattice are compared with the solutions of equations (2), (4) and (8). The numerical solution of equation (2) is obtained with a finite difference approximation with constant grid spacing δx and implicit Euler stepping with constant time steps δt [28]. Picard linearization, with absolute error tolerance ϵ, is used to solve the resulting nonlinear algebraic systems. The numerical solution of equations (4) and (8) are obtained using a fourth order Runge Kutta method with constant time step δt [18]. All numerical results presented in this work are obtained using values of δx, δt and ϵ chosen to be sufficiently small so that the numerical results are grid independent.

For all cases of extreme ($\sigma = 0.95$) and strong ($\sigma = 0.80$) adhesion shown in Figures 2–3, the solution of equation (2) is discontinuous (Figures 2–3 (d), (j)). These discontinuities are associated with $D(c)$ becoming negative for a region of c [10, 11, 29]. In this regime the pde fails to predict the discrete profiles which appear to be smooth. For modest ($\sigma = 0.65$) adhesion the solution of equation (2) remains smooth since $D(c) > 0$ (Figures 2–3 (p)). For modest adhesion the accuracy of equation (2) is much higher relative to the strong ($\sigma = 0.80$) and extreme ($\sigma = 0.95$) adhesion cases. Although equation (2) performs better for $\sigma = 0.65$, we still observe that equation (2) slightly overestimates the peak density at $t = 1000$ (Figure 2 (p)).

When $D(c)$ becomes negative for a region of c, the solution of equation (2) is qualitatively different from the solution when $D(c)$ is always positive. When $D(c)$ is always positive, equation (2) is uniformly parabolic and satisfies the usual maximum principle. This means that the solution is bounded by the initial condition so that, in our case, $c(x,t) \leq 1$ for all $t > 0$ [29, 30]. Con-

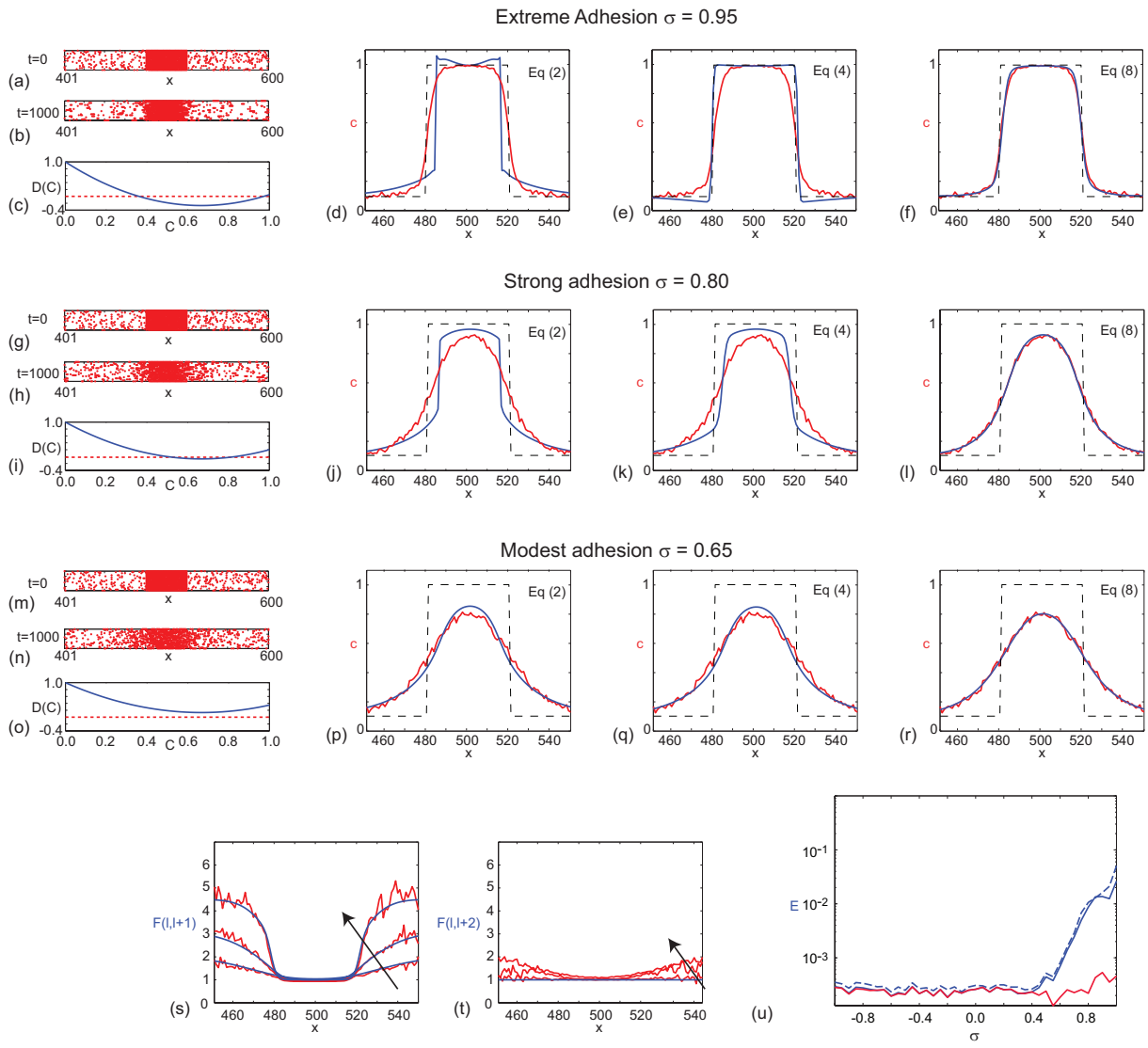

FIG. 2: (Color online). Mean-field and discrete results for a range of adhesive strengths: (a)–(f) extreme adhesion ($\sigma = 0.95$), (g)–(l) strong adhesion ($\sigma = 0.80$) and (m)–(r) modest adhesion ($\sigma = 0.65$). ((a)–(b), (g)–(h), (m)–(n)) For each adhesive strength, two snapshots of the discrete process are shown at $t = 0$ and $t = 1000$, respectively. All discrete results correspond to $\Delta = \tau = 1$, simulations are performed on a lattice with $1 \leq x \leq 1000$ and periodic boundary conditions. Discrete snapshots show 20 identically prepared realizations of the same one-dimensional process in the region $401 \leq x \leq 600$. ((d), (j), (p)) Comparisons of averaged density profiles (red), the initial condition (black dashed) and the solution of equation (2) (blue). ((e), (k), (q)) Comparisons of averaged density profiles (red), the initial condition (black dashed) and the solution of equation (4) (blue). ((f), (l), (r)) Comparisons of averaged density profiles (red), the initial condition (black dashed) and the solution of equation (8) (blue). All discrete simulation results and mean-field solutions were obtained using periodic boundary conditions. ((c), (i), (o)) Shows the nonlinear diffusivity function, $D(c) = 1 - \sigma c(4 - 3c)$, associated with equation (2). Results for extreme ($\sigma = 0.95$) and strong ($\sigma = 0.80$) adhesion show that $D(c)$ becomes negative in some interval $c \in [c_1, c_2]$ while results for the modest adhesion ($\sigma = 0.65$) show that $D(c) > 0$ for all $c \in [0, 1]$. ((s), (t)) Compare continuum (blue) and discrete (red) profiles of $F(l, l + 1)$ and $F(l, l + 2)$, respectively. In each plot, profiles of the correlation function are given for extreme ($\sigma = 0.95$), strong ($\sigma = 0.80$) and modest adhesion ($\sigma = 0.65$) with the arrow showing the direction of increasing σ. (u) The error profile, E, as a function of the adhesion parameter $\sigma \in [-1, 1]$, at $t = 1000$. Error profiles are given for equations (2) (blue dashed), (4) (blue) and (8) (red). All numerical solutions of equation 2 correspond to $\delta x = 0.2$, $\delta t = 0.01$ and $\epsilon = 1 \times 10^{-6}$. All numerical solutions of equations (4) and (8) correspond to $\delta t = 0.05$.

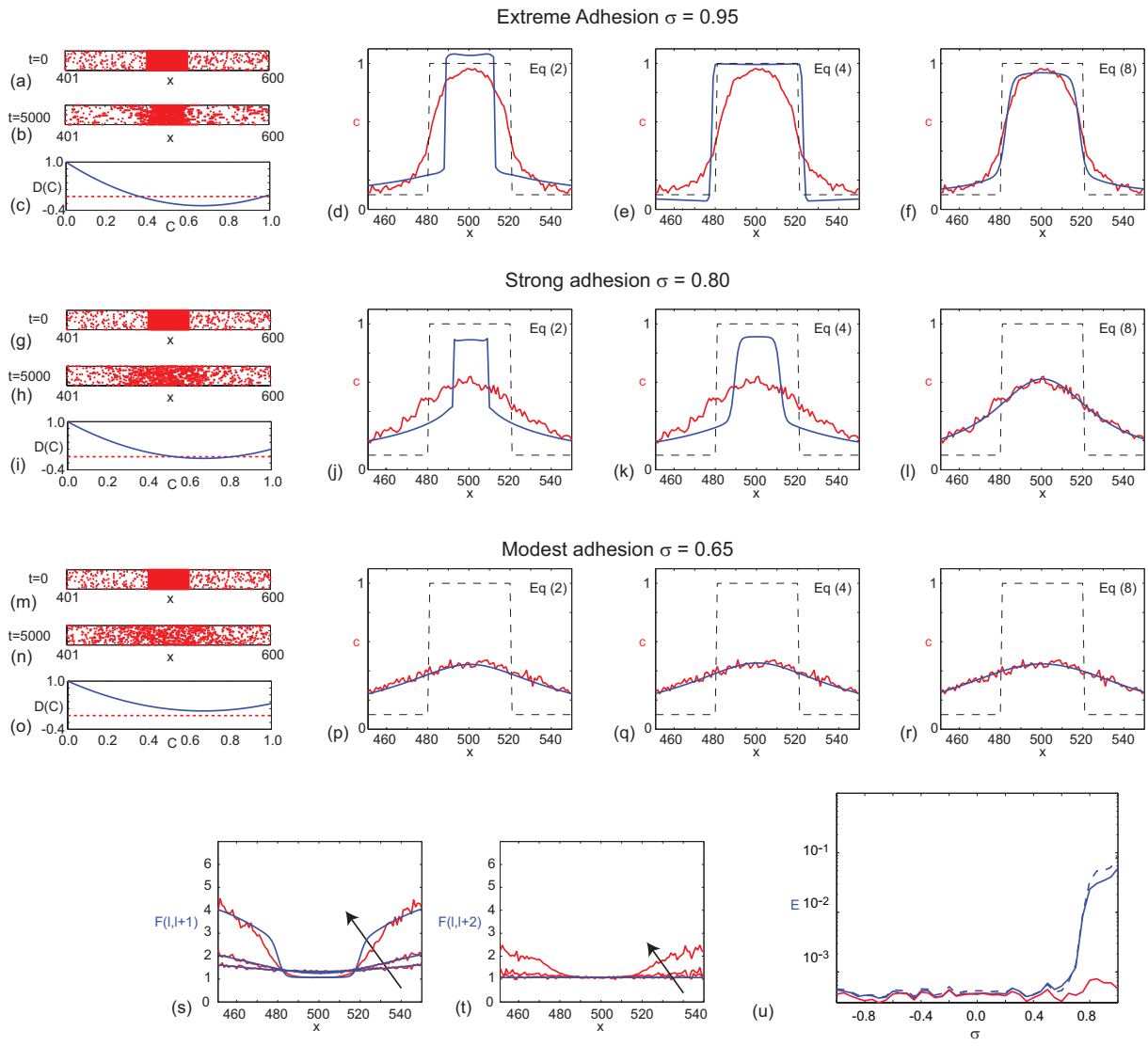

FIG. 3: (Color online). Mean-field and discrete results for a range of adhesive strengths: (a)–(f) extreme adhesion ($\sigma = 0.95$), (g)–(l) strong adhesion ($\sigma = 0.80$) and (m)–(r) modest adhesion ($\sigma = 0.65$). ((a)–(b), (g)–(h), (m)–(n)) For each adhesive strength, two snapshots of the discrete process are shown at $t = 0$ and $t = 5000$, respectively. All discrete results correspond to $\Delta = \tau = 1$, simulations are performed on a lattice with $1 \leq x \leq 1000$ and periodic boundary conditions. Discrete snapshots show 20 identically prepared realizations of the same one-dimensional process in the region $401 \leq x \leq 600$. ((d), (j), (p)) Comparisons of averaged density profiles (red), the initial condition (black dashed) and the solution of equation (2) (blue). ((e), (k), (q)) Comparisons of averaged density profiles (red), the initial condition (black dashed) and the solution of equation (4) (blue). ((f), (l), (r)) Comparisons of averaged density profiles (red), the initial condition (black dashed) and the solution of equation (8) (blue). All discrete simulation results and mean-field solutions were obtained using periodic boundary conditions. ((c), (i), (o)) Shows the nonlinear diffusivity function, $D(c) = 1 - \sigma c(4 - 3c)$, associated with equation (2). Results for extreme ($\sigma = 0.95$) and strong ($\sigma = 0.80$) adhesion show that $D(c)$ becomes negative in some interval $c \in [c_1, c_2]$ while results for the modest adhesion ($\sigma = 0.65$) show that $D(c) > 0$ for all $c \in [0, 1]$. ((s), (t)) Compare continuum (blue) and discrete (red) profiles of $F(l, l + 1)$ and $F(l, l + 2)$, respectively. In each plot, profiles of the correlation function are given for extreme ($\sigma = 0.95$), strong ($\sigma = 0.80$) and modest adhesion ($\sigma = 0.65$) with the arrow showing the direction of increasing σ. (u) The error profile, E, as a function of the adhesion parameter $\sigma \in [-1, 1]$, at $t = 5000$. Error profiles are given for equations (2) (blue dashed), (4) (blue) and (8) (red). All numerical solutions of equation 2 correspond to $\delta x = 0.2$, $\delta t = 0.01$ and $\epsilon = 1 \times 10^{-6}$. All numerical solutions of equations (4) and (8) correspond to $\delta t = 0.05$.

versely, when $D(c)$ becomes negative for a region of c, equation (2) is not uniformly parabolic and does not satisfy the usual maximum principle. This means that $c(x,t)$ may become greater than the initial condition as the profile evolves (Figures 2–3 (d)). Similar behavior has been observed previously in a different context. DiCarlo [31] used a nonlinear diffusion equation, called Richards' equation, to study fluid flow through a partially saturated porous medium. This previous work showed that the infiltration front was monotone and never increased above the long-term saturation level whenever the nonlinear diffusivity function was always positive. Similar to our results, DiCarlo showed that when the nonlinear diffusivity function contained a negative region the infiltration front became nonmonotone, and the saturation level at the leading edge increased above the long-term saturation level meaning that the governing equation no longer satisfied the usual maximum principle.

Comparing the averaged discrete profiles and the solution of equation (4) indicates that this model predicts smooth profiles, however these profiles do not accurately predict the discrete density data for strong ($\sigma = 0.80$) and extreme ($\sigma = 0.95$) adhesion (Figures 2–3 (e), (k)). Alternatively, solution of equation (8) predicts smooth profiles that are accurate, even for strong ($\sigma = 0.80$) and extreme ($\sigma = 0.95$) adhesion (Figures 2–3 (f), (l)). These results provide us with a qualitative indication of the relative roles of the assumptions underlying equation (2). We see that equation (4), without truncation, provides a modest improvement over equation (2), whereas equation (8), with no truncation or independence assumptions, provides a major improvement relative to equation (2). This indicates that the key assumption leading to the failure of equation (2) is the independence assumption.

The moment closure model (equation (8)) also provides us with a quantitative measure of the role of correlation effects through the correlation functions, shown in Figures 2-3 (s)–(t). Our results show that $F(l,l+1)$ increases with σ, confirming that correlation effects increases with increasing adhesion, and we see that the continuum $F(l,l+1)$ profiles predict the discrete values quite well at both $t = 1000$ (Figure 2 (s)) and $t = 5000$ (Figure 3 (s)). We also present discrete estimates of $F(l,l+2)$ (Figures 2–3 (t)) which are neglected in our moment closure results since we set $F(l,l+2) = 1$. Comparing profiles of $F(l,l+1)$ and $F(l,l+2)$ show that nearest neighbor correlation effects are more pronounced than then next nearest neighbor correlation effects. Our neglect of next nearest neighbor correlation effects in the moment closure model appears reasonable given the quality of match between the discrete data and the solution of equation (8).

To quantify the accuracy of equations (2), (4) and (8), we use an error norm given by

$$E = \frac{1}{100} \sum_{l=451}^{l=550} (c_l - MF(x,t))^2, \tag{15}$$

where $MF(x,t)$ is the density predicted by one of equations (2), (4) or (8), and c_l is the average density at site l from the averaged discrete simulations. We calculate E using sites in the region $451 \leq l \leq 550$ since the details of the evolved density profiles in Figures 2–3 are localized in this region. Figures 2–3 (u) compare the accuracy of equations (2), (4) and (8) for the entire range of the adhesion parameter $\sigma \in [-1, 1]$, showing that the error varies over two orders of magnitude. For all cases of repulsive motion ($\sigma < 0$), and mildly adhesive motion ($0 < \sigma < 0.5$), equations (2), (4) and (8) perform similarly we see that the solution of each mean-field model accurately matches the discrete profiles. This is is consistent with previous research [11]. For modest to extreme adhesion ($0.50 \leq \sigma \leq 1.0$), equations (2) and (4) become very inaccurate, while equation (8) continues to make accurate predictions for all $\sigma \in [-1, 1]$.

Comparing the performance of equations (2), (4) and (8) in Figure 2 at $t = 1000$ with the results in Figure 3 at $t = 5000$ indicates that the same qualitative trends are apparent at both time points. The profiles at $t = 1000$ (Figure 2) for extreme adhesion ($\sigma = 0.95$) and strong adhesion ($\sigma = 0.80$) show that the density profiles have not changed much from the initial distribution, while the results for moderate adhesion ($\sigma = 0.65$) show that the density profile has spread out much further along the lattice by $t = 1000$. The profiles at $t = 5000$ (Figure 3) for strong adhesion ($\sigma = 0.80$) show that the density profile has spread much further across the lattice, and the results for moderate adhesion ($\sigma = 0.65$) show that the density profile is almost horizontal by $t = 5000$. Since our work is motivated by studying cell migration assays, which are typically conducted over relatively short time periods, it is appropriate for us to focus on relatively short simulations so that we can examine the transient response of the system and investigate how the shape of the initial condition changes. Our results for extreme adhesion $(\sigma = 0.95)$ indicate that these profiles do not change much during the timescale of the simulations whereas our results for strong $(\sigma = 0.80)$ and moderate $(\sigma = 0.65)$ adhesion show that the profiles change dramatically during the timescale of the simulations. It is important that we consider this range of behaviors since similar observations are often made in cell migration experiments where certain cell types do not migrate very far over some time periods, whereas other cell types migrate over much larger distances during the same time period [32]. One hypothesis that might explain these experimental results is that certain cell types are affected by cell-to-cell adhesion much more than other cell types [32]. The key

result of our work is to show that the usual mean-field model, given by equation (2), is unable to describe the discrete data for strong and extreme adhesion at any time point. This is significant because many previous studies have derived traditional mean-field pde models which suffer from the same limitations as equation (2). None of these previous studies have presented any alternative mean-field models that can predict the averaged discrete profiles when contact effects dominate [6, 8, 11, 12, 14].

Although all density profiles shown in Figures 2–3 correspond to adhesion ($\sigma > 0$), we also generated similar profiles over the entire range of the parameter $\sigma \in [-1, 1]$ to obtain the error profile in Figures 2–3 (u). Results for $\sigma < 0$ correspond to agent repulsion [11] and the contact effects act to increase the rate at which the density profile smooths with time. In this context, results with $\sigma < 0$ are less interesting since $D(c)$ is always positive and agent clustering does not occur. Furthermore, equation (2) appears to make accurate predictions for all cases of repulsion. Therefore, we choose to present snapshots and detailed comparisons in Figures 2–3 for adhesion cases only ($\sigma > 0$).

Our comparisons of equations (2), (4) and (8) in Figures 2–3 were for an initial condition (equation (14)) where the average occupancy of sites was either $c(x, 0) = 0.1$ or $c(x, 0) = 1.0$ with a sharp discontinuity between these two values. We chose this initial condition because equation (2) is well-posed since the initial condition jumps across the region where $D(c)$ is negative. With $\sigma > 0.75$, $D(c)$ in equation (2) contains a region $c \in [c_1, c_2]$ where $D(c) < 0$ ($0 < c_1 < c_2 < 1$) and it is only possible to solve equation (2) when the initial condition is chosen such that $c(x, 0)$ is not in the interval $[c_1, c_2]$ [29]. Had we chosen an initial condition that did not obey these restrictions, equation (2) would be ill-posed with no solution [29]. For completeness, we now consider a second set of results for a different initial condition given by

$$c(x, 0) = 0.1 + 0.9 \exp\left[\frac{-(x - 500)^2}{400}\right]. \tag{16}$$

This initial condition is Gaussian-shaped and accesses all values of $0.1 \leq c(x, 0) \leq 1$. For values of $\sigma > 0.75$, this initial condition does not jump across the region where $D(c)$ is negative which means that equation (2) is ill-posed and we cannot obtain a solution [13, 29]. Regardless of this complication with equation (2), we repeated all simulations shown previously in Figures 2–3 with the Gaussian-shaped initial condition and we report the results in Figures 4–5 at $t = 1000$ and $t = 5000$, respectively.

Results in Figures 4–5 show the exact same qualitative trends that were illustrated previously in

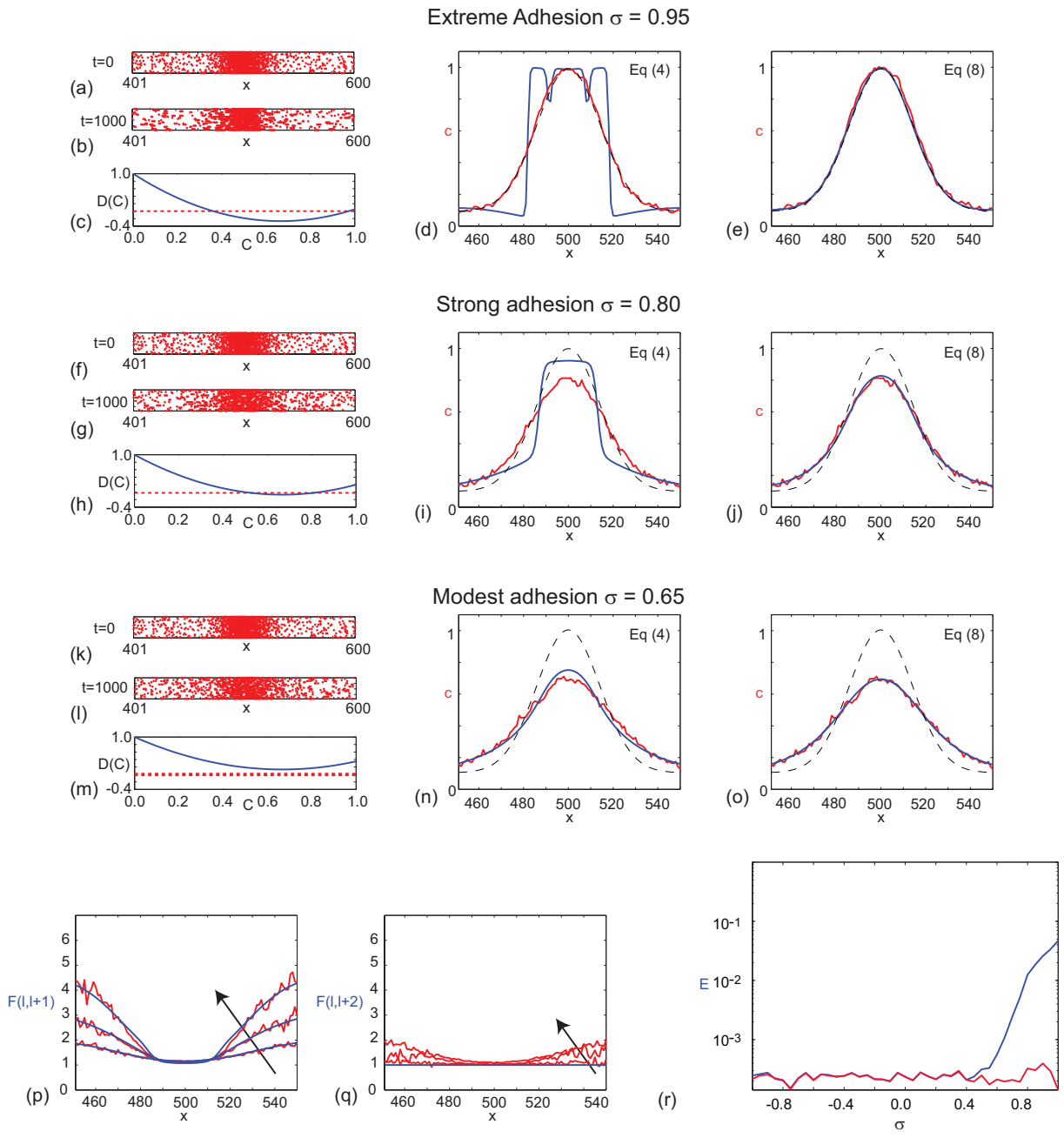

FIG. 4: (Color online). Mean-field and discrete results for a range of adhesive strengths: (a)–(e) extreme adhesion ($\sigma = 0.95$), (f)–(j) strong adhesion ($\sigma = 0.80$) and (k)–(o) modest adhesion ($\sigma = 0.65$). ((a)–(b), (f)–(g), (k)–(l)) For each adhesive strength, two snapshots of the discrete process are shown at $t = 0$ and $t = 1000$, respectively. All discrete results correspond to $\Delta = \tau = 1$, simulations are performed on a lattice with $1 \leq x \leq 1000$ and periodic boundary conditions. Discrete snapshots show 20 identically prepared realizations of the same one-dimensional process in the region $401 \leq x \leq 600$. ((d), (i), (n)) Comparisons of averaged density profiles (red), the initial condition (black dashed) and the solution of equation (4) (blue). ((e), (j), (o)) Comparisons of averaged density profiles (red), the initial condition (black dashed) and the solution of equation (8) (blue). All discrete simulation results and mean-field solutions were obtained using periodic boundary conditions. ((c), (h), (m)) show the nonlinear diffusivity function, $D(c) = 1 - \sigma c(4 - 3c)$, associated with equation (2). Results for extreme ($\sigma = 0.95$) and strong ($\sigma = 0.80$) adhesion show that $D(c)$ becomes negative in some interval $c \in [c_1, c_2]$ while results for the modest adhesion ($\sigma = 0.65$) show that $D(c) > 0$ for all $c \in [0, 1]$. ((p), (q)) Compare continuum (blue) and discrete (red) profiles of $F(l, l+1)$ and $F(l, l+2)$, respectively. In each plot, profiles of the correlation function are given for extreme ($\sigma = 0.95$), strong ($\sigma = 0.80$) and modest adhesion ($\sigma = 0.65$) with the arrow showing the direction of increasing σ. (r) The error profile, E, as a function of the adhesion parameter $\sigma \in [-1, 1]$, at $t = 1000$. Error profiles are given for equations (4) (blue) and (8) (red). All numerical solutions of equation 2 correspond to $\delta x = 0.2$, $\delta t = 0.01$ and $\epsilon = 1 \times 10^{-6}$. All numerical solutions of equations (4) and (8) correspond to $\delta t = 0.05$.

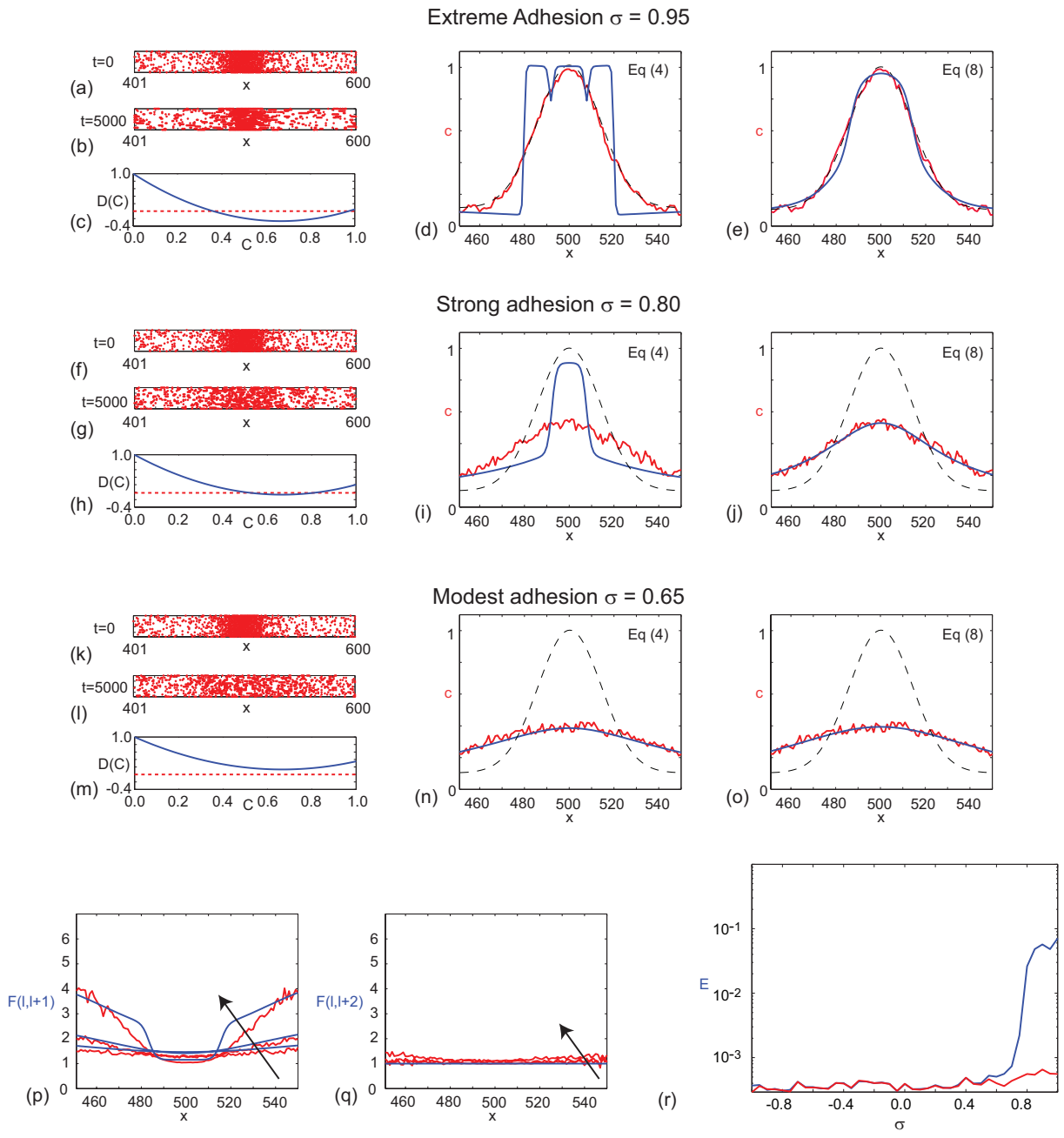

FIG. 5: (Color online). Mean-field and discrete results for a range of adhesive strengths: (a)–(e) extreme adhesion ($\sigma = 0.95$), (f)–(j) strong adhesion ($\sigma = 0.80$) and (k)–(o) modest adhesion ($\sigma = 0.65$). ((a)–(b), (f)–(g), (k)–(l)) For each adhesive strength, two snapshots of the discrete process are shown at $t = 0$ and $t = 5000$, respectively. All discrete results correspond to $\Delta = \tau = 1$, simulations are performed on a lattice with $1 \leq x \leq 1000$ and periodic boundary conditions. Discrete snapshots show 20 identically prepared realizations of the same one-dimensional process in the region $401 \leq x \leq 600$. ((d), (i), (n)) Comparisons of averaged density profiles (red), the initial condition (black dashed) and the solution of equation (4) (blue). ((e), (j), (o)) Comparisons of averaged density profiles (red), the initial condition (black dashed) and the solution of equation (8) (blue). All discrete simulation results and mean-field solutions were obtained using periodic boundary conditions. ((c), (h), (m)) show the nonlinear diffusivity function, $D(c) = 1 - \sigma c(4 - 3c)$, associated with equation (2). Results for extreme ($\sigma = 0.95$) and strong ($\sigma = 0.80$) adhesion show that $D(c)$ becomes negative in some interval $c \in [c_1, c_2]$ while results for the modest adhesion ($\sigma = 0.65$) show that $D(c) > 0$ for all $c \in [0, 1]$. ((p), (q)) Compare continuum (blue) and discrete (red) profiles of $F(l, l+1)$ and $F(l, l+2)$, respectively. In each plot, profiles of the correlation function are given for extreme ($\sigma = 0.95$), strong ($\sigma = 0.80$) and modest adhesion ($\sigma = 0.65$) with the arrow showing the direction of increasing σ. (r) The error profile, E, as a function of the adhesion parameter $\sigma \in [-1, 1]$, at $t = 5000$. Error profiles are given for equations (4) (blue) and (8) (red). All numerical solutions of equation 2 correspond to $\delta x = 0.2$, $\delta t = 0.01$ and $\epsilon = 1 \times 10^{-6}$. All numerical solutions of equations (4) and (8) correspond to $\delta t = 0.05$.

Figures 2–3. For modest adhesion $(\sigma = 0.65)$ we see that equations (4) and (8) perform similarly and both mean-field models predict the averaged discrete data accurately (Figures 4–5 (n), (o)). For strong $(\sigma = 0.80)$ and extreme adhesion $(\sigma = 0.85)$ we see that equation (4), which neglects correlation effects, is unable to predict the averaged discrete data at either $t = 1000$ or $t = 5000$ (Figures 4–5 (d), (i)) whereas equation (8) leads to an accurate mean-field prediction in all cases considered here. Comparing discrete estimates of $F(l, l+1)$ with those predicted using the moment closure model shows that the moment closure approach captures nearest neighbor correlation effects accurately (Figures 4–5 (p)), and we see that next nearest neighbor correlation effects are less pronounced than nearest neighbor correlation effects. The differences in the performance of equations (4) and (8) are quantified in terms of the error norm (equation (15)) in Figures 4–5 (r).

V. CONCLUSION

Our analysis shows it is possible to make accurate mean-field predictions of a discrete exclusion process with strong adhesion. This is important since all previous mean-field predictions are valid for mild contact effects only [6–8, 11, 12, 14]. Identifying and quantifying why traditional mean-field models fail to predict highly adhesive motion requires new approaches that relax the assumptions underlying the traditional approach. Our suite of mean-field models allow us to quantify the accuracy of assumptions relating to spatial truncation effects, and the neglect of correlation effects. We find that the traditional pde is extremely sensitive to the neglect of correlations.

The model presented in this work is a simplified model of cell migration since it deals only with one-dimensional motion without cell birth and death processes. Our previous work on moment closure models has shown how to incorporate cell birth and death processes, as well as showing that it is possible to develop moment closure models in higher dimensions. These additional details could also be incorporated into the current model. Other extensions to the discrete model include studying adhesive migration where we explicitly account for agent shape and size effects [33], or the study of adhesive migration on a growing substrate [34]. We anticipate that accurate mean-field models of these these extensions will require a similar, but more detailed, moment closure approach.

VI. ACKNOWLEDGEMENTS

We acknowledge support from Emeritus Professor Sean McElwain, the Australian Research Council project DP0878011, and the Australian Mathematical Sciences Institute for a summer vacation scholarship to Mr Stuart T Johnston.

[1] Kendall K. Molecular adhesion and its applications. (Kluwer, New York, 2004).

[2] Haye H, Wolf DE. The physics of granluar media. (Wiley-VCH, Weinheim 2006).

[3] Wolpert L. Principles of development. (Oxford University Press, Oxford 2002).

[4] Weinberg RA. The biology of cancer. (Garland Science, New York 2007).

[5] Liggett TM. Stochastic interacting systems: contact, voter and exclusion processes (Springer, New York, 1999).

[6] Deroulers C, Aubert M, Badoual M, Grammaticos B. Phys Rev E. **79** 031917 (2009).

[7] Khain E, Katakowski M, Hopkins S, Szalad A, Zheng X, Jiang F, Chopp M. Phys Rev E. **83** 031920 (2011).

[8] Simpson MJ, Towne C, McElwain DLS, Upton Z. Phys Rev E. **82** 041901 (2010).

[9] Khain E, Sander L, Schneider-Mizell CM. J Stat Phys. **128** 209 (2007).

[10] Anguige K, Schmeiser C. J Math Biol. **58** 395 (2009).

[11] Fernando AE, Landman KA, Simpson MJ. Phys Rev E. **81** 011903 (2010).

[12] Penington C, Hughes BD, Landman KA. Phys Rev E. **84**, 041120 (2011).

[13] Simpson MJ, Landman KA, Hughes BD, Fernando AE. Physica A. **389** 1412 (2009).

[14] Landman KA, Fernando AE. Physica A. **390** 3742 (2011).

[15] Chowdhury D, Schadschneider S, Nishinari K. Phys Life Rev. **2** 318 (2005).

[16] Codling EA, Plank MJ, Benhamou S. J Royal Soc Interface. **5** 813 (2008).

[17] Baker RE, Simpson MJ. Phys Rev E. **82** 041905 (2010).

[18] Simpson MJ, Baker RE. Phys Rev E. **83** 051922 (2011).

[19] Mai J, Kuzovkov NV, von Niessen W. J Chem Phys. **98** 10017 (1993).

[20] Mai J, Kuzovkov NV, von Niessen W. Physica A. **203** 298 (1994).

[21] Law R, Murrell DJ, Dieckmann U. Ecology. **84** 252 (2003).

[22] Murrell DJ, Dieckmann U, Law R. J Theor Biol. **229** 421 (2004).

[23] Raghib M, Hill NA, Dieckmann U. J Math Biol. **62** 605 (2011).

[24] Singer A. J Chem Phys. **121** 3657 (2004).

[25] Sharkey KJ. J Math Biol. **57** 311 (2008).

[26] Dangerfield CE, Ross JV, Keeling MJ. J Royal Soc Interface. **6** 761 (2009).

[27] Seki K, Tachiya M. Phys Rev E. **80** 041120 (2009).

[28] Simpson MJ, Landman KA, Clement TP. Math Comput Simulat. **70** 44 (2005).

[29] Witelski TP. Appl Math Lett. **8** 27 (1995).

[30] Protter MH, Weinberger HF. Maximum principles in differential equations. (Prentice-Hall, New Jersey, 1967).

[31] DiCarlo DA, Juanes R, LaForce T, Witelski TP. Water Resour Res. **44** W02406 (2008).

[32] Kam Y, Guess C, Estrada L, Weidow B, Quaranta V. BMC Cancer. **8** 198 (2008).

[33] Simpson MJ, Baker RE, McCue SW. Phys Rev E. **83** 021901 (2011).

[34] Binder BJ, Landman KA, Simpson MJ, Mariani M, Newgreen DF. Phys Rev E. **78** 031912 (2008).